Table 2. New compression fractures within 1 month.

Patient	Sex	Age, years	PVP performed on vertebral bodies	Analyzed vertebral bodies	Newly developed vertebral body fracture after PVP
A	M	76	L2, L3	L1, L4	L1: new fracture
B	F	66	TH12, L1, L2, L3	Th11, L4	L4: new fracture
C	F	74	Th11, Th12, L1	Th10, L2	L2: new fracture
D	F	76	Th6, Th8	Th9	Th9: new fracture
E	F	79	Th12	Th11, L1	L1: new fracture
F	M	66	L1	Th12, L2	Th12: new fracture
G	M	54	L1	Th12, L2	
H	F	70	Th12	Th11, L1	
I	F	69	Th12, L1, L2	Th11, L3	
J	F	64	L1, L2	L3	
K	F	80	Th12, L3	L1	
L	F	76	L1, L4	L2, L3, L5	
M	F	69	Th12, L1, L3	L2, L4	
N	F	72	L3	L2, L4	
O	F	70	L4, L5	L3	
P	F	71	L1, L2, L3	Th12, L4	
Q	F	84	L3	L2, L4	
R	F	76	Th11, Th12, L1, L2	Th10	
S	F	78	L1, L4, L5	Th12, L2, L3	
T	F	63	Th12	Th11, L1	
U	F	79	Th11, Th12, L3	L1, L2, L4	
V	F	71	Th12, L4, L5	Th11, L3	
W	F	71	Th12, L1, L3	Th11, L2, L4	
X	F	78	Th9, Th12, L1	Th11, L2	L4: new fracture not adjacent vertebral body
Y	F	74	Th12, L1	Th11, L2	
($n=25$)	3 M, 22 F	72.2±6.5	56 (20 Th, 36 L)	49 (16 Th, 33 L)	7 (2 Th, 5 L)

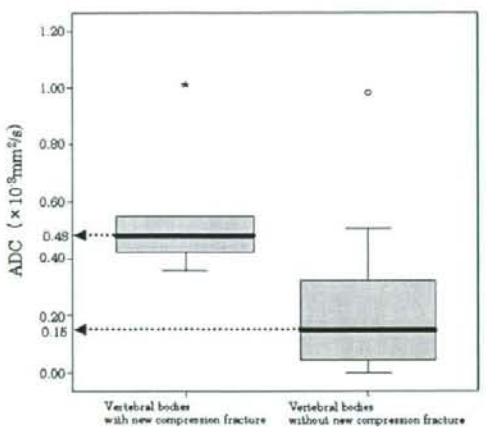

Fig. 2. Mean ADC for individual vertebrae before PVP. Mean ADC for vertebral bodies with a new compression fracture was 0.55×10^{-3} mm^2/s (range 0.36–1.01×10^{-3} mm^2/s, median value 0.48×10^{-3} mm^2/s). In contrast, mean ADC for vertebral bodies without a new compression fracture was 0.20×10^{-3} mm^2/s (range 0–0.98×10^{-3} mm^2/s, median value 0.15×10^{-3} mm^2/s). Statistically significant differences were noted between the two groups ($P < 0.001$).

before PVP and 0.24×10^{-3} mm^2/s (range 0–0.82×10^{-3} mm^2/s) after PVP, and no statistically significant difference was apparent.

Discussion

According to past studies that followed patients for more than 6 months after PVP, the incidence of new compression fractures varies widely from 0 to 50% (4, 16–20). Uppin et al. reported an incidence of 12.5%, and noted that 67% of these were adjacent-level fractures (4). Two hypotheses have been proposed for the onset of a new compression fracture: 1) onset of a new compression fracture is unrelated to PVP (21); and 2) onset of a new compression fracture in adjacent vertebral bodies is high because cement injection increases the strength of the treated vertebral bodies, resulting in a relative weakening of untreated vertebral bodies (22, 23). Furthermore, new compression fractures tend to occur at adjacent levels (2–4) relatively soon after PVP (4). However, whether new compression fractures are attributable to PVP or a natural course of osteoporosis remains unclear at present.

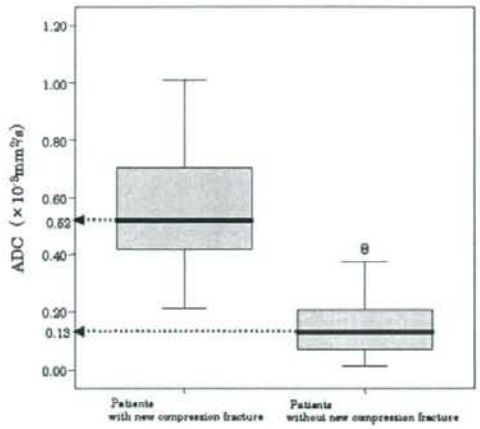

Fig. 3. ADC for each patient before PVP. Mean ADC for the six patients with new compression fractures was 0.55×10^{-3} mm^2/s (range 0.21–1.01 $\times 10^{-3}$ mm^2/s, median value 0.52×10^{-3} mm^2/s), while that for the 19 patients without new compression fractures was 0.17×10^{-3} mm^2/s (range 0.01–0.43 $\times 10^{-3}$ mm^2/s, median value 0.13×10^{-3} mm^2/s). Statistically significant differences existed between the two groups ($P < 0.001$).

In our study, new compression fractures were seen in seven of the 25 patients (28%). Since patients were followed for 1 month, this figure was higher than reported in previous studies (4, 16–20). Reasons for this could have been that one study defined new fractures as compression fractures seen on plain radiography taken when patients returned to hospital with recurrent back pain following PVP (4), while some prospective follow-up studies (3, 24) based diagnoses solely on conventional radiography. In the present study, the definition of a new compression fracture emphasized clinical features: even if the degree of decrease in vertebral height on plain radiography was minute, patients were diagnosed with new compression fractures if pain on percussion of the vertebral spinous process and a bone marrow edema pattern as assessed by MRI were observed. These criteria were utilized to ascertain whether additional PVP was required at the time of assessment.

Prophylactic PVP is currently contraindicated for vertebral bodies without compression fractures (25), but research on prophylactic PVP has been conducted in recent years (26, 27). If the risk of a new compression fracture can be evaluated accurately and vertebral bodies at higher risk for compression fractures can be identified, use of prophylactic PVP may be justified. At present, PVP is performed to treat vertebral bodies with compression fractures, and is thus only performed on patients with an existing compression fracture. According to one study, up to 25% of patients with compression fractures develop new compression fractures within 1 year (12). As mentioned above, new compression fractures after PVP are likely to occur at adjacent levels, and vertebral bodies adjacent to vertebral bodies treated by cement injection thus appear to be at higher risk for new compression fracture.

Diffusion in a microscopic sense is a phenomenon dependent on the random or Brownian motion of individual molecules. MRI can be made sensitive to diffusion of tissue water molecules, when very strong bipolar gradient pulses are inserted into either a spin-echo pulse sequence (STEJSKAL and TANNER technique) (28) or a gradient-echo pulse sequence (10). As far as the random motion of water molecules is concerned, because size and direction change markedly depending on temperature and surrounding environment, microscopic cellular conditions can be ascertained by examining the diffusion of water molecules. The number of protons gives the intensity of the MRI signal, and their motion because of thermal diffusion gives the ADC. In normal vertebral bodies, barely any mobile free water is present in the interstitial space. As a result, with the echo-planar imaging (EPI) pulse sequence used in the present study, fat signals are suppressed to resolve the issue of chemical-shift artifacts. Subsequently, in normal vertebral bodies, the number of mobile protons generating signals on MRI is very low, resulting in very low ADC. Conversely, high ADC indicates large numbers of mobile protons, suggesting mobile free water in the interstitial space, or tumor cells in bone marrow. The ADC of vertebral bodies with benign fractures is higher than that of normal vertebral bodies because of an increase in interstitial space caused by edema or hemorrhage (10, 12, 14). MIKAMI et al. reported that an area with exudate and neutrophil infiltration in a vertebral body was recognized as a high ADC area in their animal experiments of bone marrow inflammation (29). Since the amount of mobile free water is likely to be high in vertebral bodies about to develop compression fractures, measuring ADC in vertebral bodies seems likely to offer a reasonable assessment of the likelihood of compression fractures. We set the b value to 1000 s/mm^{-2}. Although the optimal b value for vertebral DWI has yet to be determined, diffusion has greater influence at higher b values such as 1000 s/mm^{-2} (12).

If PVP itself were involved in the onset of new adjacent-level fractures, the significance of preventative PVP would clearly be lost. Therefore, to ascertain the effects of PVP on adjacent vertebral bodies, ADCs were compared before and after PVP. The results showed no statistically significant differences in ADC before and after the procedure. From these results, PVP does not induce inflammation because of no increase of mobile free water. However, the influence of PVP on an adjacent vertebral body also includes biomechanical factors, and we were not able to conclude that PVP itself does not affect the incidence of new adjacent vertebral compression fractures.

In the present study, ADC was only measured using the EPI pulse sequence in DWI. EPI allows DWI to be performed in a short period of time, and since all necessary data for a single image can be gathered from a single radiofrequency excitation, the effects of motion artifacts are low. However, EPI is very sensitive to susceptibility effects, which therefore represent a major concern. Reducing these artifacts requires use of a high-receiver bandwidth or radiofrequency (RF) coil with cylindrical geometry, such as a body coil (10). However, the present study used a quadrature detection thoracolumbar spine coil with a moderate receiver bandwidth. Using EPI, susceptibility artifacts are substantially suppressed by using shorter time for signal sampling. This can be achieved by the parallel imaging technique. However, we did not use parallel imaging. Sufficient measures against susceptibility effects were thus not enforced, and this represents a significant limitation to the present study. Future investigations will require measurement of ADC using line scanning.

The results of this study suggest the possibility of predicting compression fractures of vertebral bodies adjacent to vertebral bodies injected with cement substance, and contribute toward clarifying the significance of prophylactic PVP. However, as only adjacent vertebral bodies were examined in a small number of subjects, these findings alone do not justify the introduction of preventative PVP.

In conclusion, the ADC of adjacent vertebral bodies as assessed by diffusion-weighted imaging before PVP might be a predictor for a new compression fracture following PVP.

Acknowledgements

We are grateful to members of the MRI group at Kansai Medical University for valuable assistance.

References

1. Galibert P, Deramond H, Rosat P, Le Gars D. Preliminary note on the treatment of vertebral angioma by percutaneous acrylic vertebroplasty [in French]. Neurochirugie 1987;33:166–8.
2. Grados F, Depriester C, Cayrolle G, Hardy N, Deramond H, Fardellone P. Long-term observations of vertebral osteoporotic fractures treated by percutaneous vertebroplasty. Rheumatology 2000;39:1410–4.
3. Perez-Higueras A, Alvarez L, Rossi RE, Quinones D, Al-Assir I. Percutaneous vertebroplasty: long-term clinical and radiological outcome. Neuroradiology 2002;44: 950–4.
4. Uppin AA, Hirsch JA, Centenera LV, Pfiefer BA, Pazianos AG, Choi IS. Occurrence of new vertebral body fracture after percutaneous vertebroplasty in patients with osteoporosis. Radiology 2003;226:119–24.
5. Evans AJ, Jensen ME, Kip KE, DeNardo AJ, Lawler GJ, Negin GA, et al. Vertebral compression fractures: pain reduction and improvement in functional mobility after percutaneous polymethylmethacrylate vertebroplasty – retrospective report of 245 cases. Radiology 2003;226:366–72.
6. Heini PF, Walchli B, Berlemann U. Percutaneous transpedicular vertebroplasty with PMMA: operative technique and early results. Eur Spine J 2000;9:445–50.
7. Hodler J, Peck D, Gilula LA. Midterm outcome after vertebroplasty: predictive value of technical and patients-related factors. Radiology 2003;227:662–8.
8. Kallmes DF, Jensen ME. Percutaneous vertebroplasty. Radiology 2003;229:27–36.
9. Mathis JM, Barr JD, Belkoff SM, Barr MS, Jensen ME, Deramond H. Percutaneous vertebroplasty: a developing standard of care for vertebral compression fractures. Am J Neuroradiol 2001;22:373–81.
10. Chan JHM, Peh WCG, Tsui EYK, Chau LF, Cheung KK, Chan KB, et al. Acute vertebral body compression fractures: discrimination between benign and malignant causes using apparent diffusion coefficients. Br J Radiol 2002;75:207–14.
11. Herneth AM, Philipp MO, Naude J, Funovics M, Beichel RR, Bammer R, et al. Vertebral metastases: assessment with apparent diffusion coefficient. Radiology 2002;225:889–94.
12. Lindsay R, Silverman SL, Cooper C, Hanley DA, Barton I, Broy SB, et al. Risk of new vertebral fracture in the year following a fracture. JAMA 2001;285:320–1.
13. Maeda M, Sakuma H, Maier SE, Takeda K. Quantitative assessment of diffusion abnormalities in benign and malignant vertebral compression fractures by line scan diffusion-weighted imaging. Am J Roentgenol 2003;181: 1203–9.
14. Zhou XJ, Leeds NE, McKinnon GC, Kumar AJ. Characterization of benign and metastatic vertebral compression fracture with quantitative diffusion MR imaging. Am J Neuroradiol 2002;23:165–70.
15. Burdette JH, Elster AD, Ricci PE. Calculation of apparent diffusion coefficients (ADCs) in brain using two-point and six-point methods. J Comput Assist Tomogr 1998;22:792–4.
16. Barr JD, Barr MS, Lemley TJ, McCann RM. Percutaneous vertebroplasty for pain relief and spinal stabilization. Spine 2000;25:923–8.

17. Cortet B, Cotton A, Boutry N. Percutaneous vertebroplasty in the treatment of osteoporotic compression fractures: an open prospective study. J Rheumatol 1999; 26:2222–8.
18. Cyteval C, Sarrabere MP, Roux JO, Thomas E, Jorgensen C, Blotman F, et al. Acute osteoporotic vertebral collapse: open study on percutaneous injection of acrylic surgical cement in 20 patients. Am J Roentgenol 1999;173:1685–90.
19. Jensen ME, Evanas AJ, Mathis JM, Kallmes DF, Cloft HJ, Dion JE. Percutaneous methylmethacrylate vertebroplasty in the treatment of osteoporotic vertebral body compression fractures: technical aspect. Am J Neuroradiol 1997;18:1897–904.
20. Zoarski GH, Snow P, Olan WJ. Percutaneous vertebroplasty for osteoporotic compression fractures: quantitative prospective evaluation of long-term outcomes. J Vasc Interv Radiol 2002;13:139–48.
21. Jensen ME, Kallmes DF, Short JG. Percutaneous vertebroplasty does not increase the risk of adjacent level fracture: a retrospective study. In: Proceedings of the American Society of Neuroradiology, Atlanta, GA, April 3–8, 2000.
22. Berlemann U, Ferguson SJ, Nolte LP, Heini PF. Adjacent vertebral failure after vertebroplasty: a biomechanical investigation. J Bone Joint Surg Br 2002;84: 748–52.
23. Polikeit A, Norte LP, Ferguson SJ. The effect of cement augmentation on the load transfer in an osteoporotic functional spinal unit: finite-element analysis. Spine 2003;28:991–6.
24. Legroux-Gerot I, Lormeau C, Boutry N, Cotton A, Duquesnoy B, Cortet B. Long-term follow-up of vertebral osteoporotic fractures treated by percutaneous vertebroplasty. Clin Rheumatol 2004;23:310–7.
25. Barr JD, Mathis JM, Barr MS, Denardo AJ, Dion JE, Guterman LR, et al. Standard for the performance of percutaneous vertebroplasty. In: American College of Radiology Standards 2000–2001. Reston, VA: American College of Radiology; 2000. p. 441–8.
26. Sun K, Liebschner MA. Biomechanics of prophylactic vertebral reinforcement. Spine 2004;29:1428–35.
27. Higgins KB, Harten RD, Langrana NA, Reiter MF. Biomechanical effects of unipedicular vertebroplasty on intact vertebrae. Spine 2003;28:1540–7.
28. Stejskal EO, Tanner JE. Spin diffusion measurements: spin echoes in the presence of time-dependent field gradient. J Chem Phys 1965;42:288–92.
29. Mikami M. Application of diffusion-weighted MR imaging to the diagnosis of bone metastasis: a fundamental study using rabbit bone tumor model. Nippon Igaku Hoshasen Gakkai Zasshi 2004;64:107–13.

The British Journal of Radiology, 82 (2009), 249–253

SHORT COMMUNICATION

Cerebral microembolisation during radiofrequency ablation of lung tumours: detection by carotid duplex ultrasound

[1]N TANIGAWA, MD, PhD, [1]S KARIYA, MD, PhD, [1]H KOJIMA, MD, [2]A KOMEMUSHI, MD, PhD, [1]Y SHOMURA, MD, PhD, [2]K IKEDA, MD, PhD, [1]N OMURA, MD, [1]T TOKUDA, MD, [1]M MAEHARA, MD, [1]J TERADA, MD and [1]S SAWADA, MD, PhD

[1]*Department of Radiology, Kansai Medical University Hirakata hospital, 2-3-1 Shinmachi, Hirakata, Osaka, 573-1191 and* [2]*Department of Radiology, Kansai Medical University Takii Hospital, 10-15 Fumizono, Moriguchi, Osaka, 570-0074, Japan*

ABSTRACT. The aim of this study was to investigate the appearance of microbubbles during radiofrequency ablation (RFA) of lung tumours. Eight consecutive patients (mean age, 73.1 years; 3 men and 5 women; 10 malignant lesions; mean lesion size, 24.8 mm) who underwent RFA of lung tumours using internally cooled single electrodes were enrolled. During the RFA procedure, the right internal carotid artery was continuously monitored by duplex ultrasound. High-intensity transient signals (HITS) that occurred in the Doppler blood flow waveform were taken to indicate microbubbles. 21 RFA applications were performed for the 10 lesions. HITS were observed in 19 of 21 RFA applications; the mean frequency in a single application was 10 ± 13.3. A statistical correlation was seen between the duration of energy deposition and the number of HITS, and between tumour size and the number of HITS. Microbubbles were detected in all patients in the late phase of the first session of RFA.

Received 2 January 2008
Revised 1 May 2008
Accepted 7 May 2008

DOI: 10.1259/bjr/10127675

In radiofrequency ablation (RFA) treatment, heat is generated in the non-insulated portion of the electrode by dielectric heating caused by radiofrequency. The heating results in coagulation necrosis of the target tissue. The circumstances of heat generation vary according to the anatomical environment of the tissue surrounding the probe tip, *e.g.* differences in the vasculature and tissue resistance and in the shape of the electrode.

Microbubbles are known to form during RFA of the liver [1–4]. When they do form during RFA of lung tumours, these microbubbles enter the pulmonary veins, and the emboli then continue into the systemic circulation via the left heart. It has been suggested that these emboli may also enter the cerebral circulation and cause cerebral complications, specifically microembolism. Microbubble formation has also been reported to occur during RFA of lung tumours, and the effect of microbubbles on the brain has been investigated by CT and MRI [5, 6]. We therefore designed a prospective study to investigate the number of microbubbles per minute during pulmonary RFA using internally cooled electrodes.

Address correspondence to: Noboru Tanigawa, Department of Radiology, Kansai Medical University Hirakata hospital, 2-3-1Shinmachi, Hirakata, Osaka, 573-1191, Japan. E-mail: tanigano@hirakata.kmu.ac.jp

Methods and materials

Patients

The study was conducted in accordance with the Declaration of Helsinki and written informed consent was obtained from all patients prior to treatment. Subjects comprised 8 consecutive patients (mean age, 73.1 years; range, 64–89 years; 3 men and 5 women; 10 lesions) who underwent RFA treatment of lung tumours. The underlying disease was primary lung cancer in four patients and metastatic lung cancer in four patients, with the primary cancers in these patients being gastric cancer, maxillary cancer, hepatocellular carcinoma and colon cancer. One primary lung cancer patient and the patient with lung metastasis of maxillary cancer had two lesions in both lungs; RFA was therefore performed twice, on different days. 10 treatments were performed for the 10 lesions, comprising 21 RFA sessions. A mean of 2.1 RFA sessions (range, 1–4 sessions) were performed for each lesion.

RFA procedure

All procedures were performed under conscious sedation. As pre-medication, 0.5 mg of atropine sulphate (Tanabe, Osaka, Japan), 25 mg of hydroxyzine hydrochloride (Pfizer Japan, Tokyo, Japan), and 10 mg of morphine hydrochloride (Sankyo, Tokyo, Japan) were administered by intramuscular injection 30 min before the procedure.

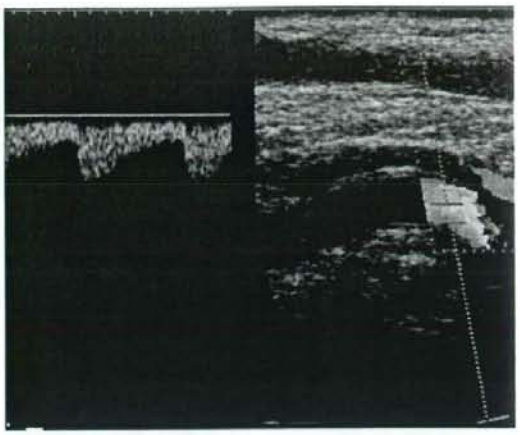

Figure 1. Duplex ultrasound image obtained during radiofrequency ablation.

The electrode used in all cases was an internally cooled single needle. The generator used was the Cool-Tip system (Radionics, Burlington, MA), with ablation performed in impedance control mode.

Two grounding pads were attached to both thighs. Unenhanced CT imaging of the area including the lesion (slice thickness, 3 mm; interval, 3 mm) was then performed; the puncture line was visualized; and local anaesthesia was performed by administering 10 cm^3 of 1% xylocaine directly beneath the parietal pleura along the puncture line using a 22-gauge Cathelin needle (Terumo Europe, Leuven, Belgium). CT imaging was repeated with the Cathelin needle used for local anaesthesia still in place. The orientation of the Cathelin needle was determined, and a 17-gauge 15 cm internally cooled single electrode (Radionics) was then advanced to the lesion site. The location of the probe in relation to the tumour was determined by CT, and the application of current was initiated. An electrode with a 2 cm non-insulated portion was used for tumours <2 cm in diameter, and an electrode with a 3 cm non-insulated portion was used for tumours ≥2 cm in diameter.

An algorithm of energy deposition was initiated at 15–30 W and was gradually increased at a rate of 10 W min^{-1}. The endpoint of one RFA application was defined as the point at which the RFA generator output automatically stopped when the impedance increased by 20 ohm compared with the initial level. At the completion of each application, CT imaging was performed and the tumour periphery was checked for the appearance of ground-glass shadow. If no ground-glass shadow was present in the tumour periphery, the puncture needle was relocated and multiple ablations were performed. The endpoint of a single procedure was defined as the appearance of ground-glass shadow in the entire region of the tumour periphery. During the ablation procedure, output, impedance and the temperature of the tip of the electrode were continuously monitored.

Immediately after the RFA treatment, unenhanced CT imaging of all lung fields (slice thickness, 5mm; interval, 15 mm) was performed, and the presence or absence of pneumothorax was determined. For 2 h after RFA, the patient rested in the supine position and underwent nasal oxygen inhalation at a rate of 2 l min^{-1}. The chest radiograph was taken in the sitting position using a portable imaging system 2 h after the ablation procedure, and the chest radiography was performed the following day to check for pneumothorax.

Monitoring of the internal carotid artery with duplex ultrasound

During the RFA procedure, the right internal carotid artery was continuously monitored by duplex ultrasonography (Figure 1). Firstly, the internal carotid artery was identified and sample points in the carotid were established by B-mode ultrasonography (Power Vision 8000; Toshiba, Tokyo, Japan). Then, the Doppler angle was aligned to the jet and kept below 60°. The pulsed Doppler gate was positioned in the centre of the common carotid artery, approximately 1–2 cm proximal to the carotid bifurcation, and a spectral waveform was obtained. The gate size was fixed on 5 mm and the velocity range was also fixed at 53.7 cm s^{-1}. Before the radiofrequency energy deposition, the Doppler blood flow waveform was monitored to determine a baseline number of high-intensity transient signals (HITS). HITS that occurred in the Doppler blood flow waveform were taken to indicate microbubbles (Figure 2). HITS were defined as follows: (i) audible high-intensity Doppler signals of brief duration; (ii) signals that were predominantly unidirectional; and (iii) signals occurring singly or, if more than one, randomly throughout the cardiac cycle.

Using a linear 7 MHz probe, monitoring was performed continuously from the time at which RFA output was initiated until 1 min after output was stopped. A super VHS video recording of the online screen was obtained for reading and analysis. HITS were confirmed

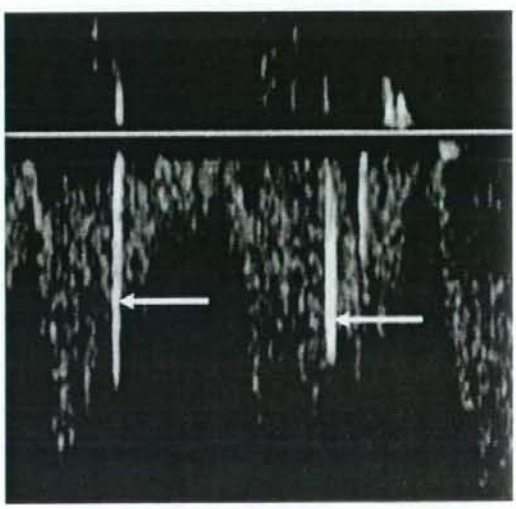

Figure 2. Pulse wave image obtained radiofrequency ablation. Visible vertical spikes (white arrows) indicating microemboli were seen.

both visually and auditorily, and the timing and frequency of their occurrence were recorded.

Data analysis

We recorded the site of RFA treatment, maximum tumour diameter, ablation time for each application, and maximum output. If multiple applications were performed for a single treatment, we also recorded whether the needle position was changed between the initial and subsequent applications.

Continuous observation for HITS was carried out from the initiation to completion of ablation in each RFA application. The number of HITS in each 1-min interval was recorded, and the total number of HITS per application was examined.

Statistical analysis

The presence or absence of a correlation between tumour size and HITS frequency and between maximum output and HITS frequency was determined using Pearson's correlation coefficient. For patients in whom RFA was performed twice at the same site for a single lesion with no change in the location of the radiofrequency probe, the difference in HITS frequency between the first and second RFA applications was tested for significance using the Wilcoxon signed-ranks test.

Results

Mean lesion size was 24.8 mm (range, 10–55 mm). For the first treatment, one patient underwent a single application, eight patients underwent two applications, and one patient underwent four applications. Among the patients who underwent multiple RFA applications, six underwent two applications for the same site without changing the needle position, and two had a change of needle position between the two applications. The remaining patient underwent four applications for the same tumour, with the same needle position used for the first and second applications; the needle position was changed for the third application, and this needle position was maintained in the fourth application. A single application took 14 min 45 s ± 0 min 45 s (range, 3 min 20 s to 47 min 12 s). Maximum radiofrequency energy output was 96.4 ± 35.5 W (range, 50–150 W).

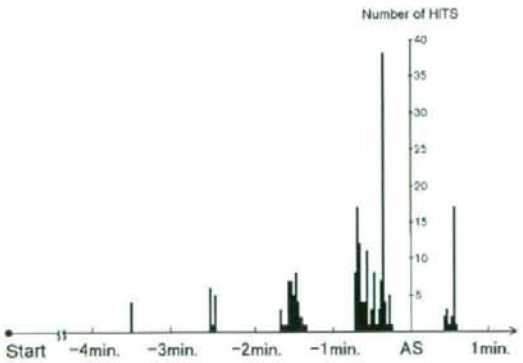

Figure 3. Graph shows the timing and frequency of high-intensity transient signals (HITS) in each case. HITS persisted for 1 min after energy was automatically shut off, and we observed a tendency towards an increasing frequency of HITS towards this shut-off. AS, automatic stop of energy deposition; Start, the start of radiofrequency energy deposition.

HITS were observed during RFA in 19 of 21 applications; the mean frequency in a single application was 10 ± 13.3 (range, 0–60; Table 1). In the two applications in which HITS did not occur (second application of lesion 1, and second application of lesion 6), we performed the second RFA application immediately after the first one, targeting the same tumour and using the same needle position. In contrast, HITS were observed in all first RFA applications of the treatment.

The timing and frequency of HITS in each case are shown in Figure 3. HITS persisted for 1 min after the energy was automatically shut off, and we observed a tendency towards an increasing frequency of HITS towards this shut-off. On average, HITS appeared 85.5 s before energy output stopped. Furthermore, as the end of the RFA application approached, we usually identified more occurrences of HITS (Figure 3). A statistical correlation was seen between the duration of energy deposition and the number of HITS (r=0.545, p=0.0095). A statistical correlation also was found between tumour size and the number of HITS (r=0.848, p=0.001). In patients who underwent multiple RFA applications at the same site, a statistically significant difference was seen between the initial application and subsequent applications with respect to the frequency of HITS (p=0.0352).

Discussion

Microbubbles can also occur during RFA of lung tumours, and to date there have been two reports of microbubble detection during this procedure [5, 6]. If they do develop, these microbubbles enter the pulmonary veins and continue into the systemic circulation via the left heart.

To detect microbubbles in the cerebral circulation, we used duplex ultrasound to ascertain HITS in the internal carotid artery. Normally, HITS monitoring of the carotid artery is used for the detection of microbubbles, and HITS are considered to represent intravascular air bubbles or thrombi [7–9]. In the present investigation, HITS were detected in 19 of 21 RFA applications, occurring in the initial RFA application in all of the patients. Thus, the findings indicated that microbubbles occurred in all patients who underwent RFA of lung tumours, as is the case with RFA of liver tumours, and that the microbubbles may have entered the systemic and cerebral circulation from the pulmonary veins via the left heart. The number of patients was small but the total number of HITS might be much greater if the true probability of HITS in all arteries was estimated. Moreover, the microbubbles tended to occur immediately before output was automatically stopped owing to an increase in impedance. This indicated that the

Table 1. A summary of results

Lesion no.	Maximum diameter (mm)	Application no.	Electrode position of each RFA application	Duration of RFA	Maximam power (watt)	Total number of HITS
1	15	1st		9 min 45 s	80	8
		2nd	Same[a]	6 min 6 s	70	0
2	30	1st		16 min 12 s	130	19
		2nd	Different[b]	17 min 43 s	130	12
3	18	1st		5 min 5 s	60	10
		2nd	Same	3 min 50 s	50	4
4	28	1st		47 min 12 s	108	23
5	20	1st		3 min 20 s	70	1
		2nd	Same	11 min 29 s	50	4
		3rd	Different	6 min 45 s	50	8
		4th	Same	9 min 9 s	50	3
6	28	1st		15 min 15 s	130	11
		2nd	Same	17 min 00 s	130	0
7	55	1st		21 min 3 s	140	19
		2nd	Different	27 min 27 s	150	60
8	10	1st		11 min 14 s	70	12
		2nd	Same	10 min 35 s	70	1
9	30	1st		18 min 28 s	126	10
		2nd	Same	17 min 45 s	130	2
10	25	1st		20 min 12 s	110	1
		2nd	Same	14 min 00 s	120	2

RFA, radiofrequency ablation; HITS, high-intensity transient signals.
[a]Same means the same electrode position as the previous ablation.
[b]Different means a different electrode position from the previous RFA application.

microbubbles occurred during the time that the temperature increase in the periphery of the radiofrequency probe was at its peak. HITS occurred for all but 2 of the 22 RFA applications. Both of these applications were the second RFA application for the same tumour, performed with no change in the location of the probe from that used at the first RFA application. A possible explanation for the absence of microbubbles in these cases is that the fluid in the periphery of the radiofrequency probe may have evaporated during the first RFA application, leaving no fluid to cause microbubbles during the second application. This indicates that the HITS that we observed may have resulted from water vapour produced by vaporization of fluid in the tissues caused by the high temperature. Rose et al [5] identified vapour formation from (i) blood and water, (ii) nitrogen or nitrous oxide gas leaving solution during tissue heating, and (iii) carbon dioxide generated from charring as possible sources of microbubbles during lung RFA.

Yamamoto et al [6] monitored the internal carotid artery by Doppler ultrasound during lung RFA and observed microbubbles with brightness-mode and/or Doppler scanning in only 3 of 17 patients. We found no microbubbles with brightness-mode scanning in any of the patients examined. However, the frequency of HITS in our investigation was clearly higher than that reported by Yamamoto et al [6]. Possible explanations for this are differences in the output of the RFA generator, and in the manner in which the tissue was ablated owing to variation in the shape of the RFA needle. Yamamoto et al [6] used a 15-gauge Leveen needle, and the difference in the shape of the non-insulated portion of the radiofrequency probe tip may have resulted in a difference in the rate of tissue temperature increase and, consequently, a different form of ablation. Moreover, the mean maximum radiofrequency output was 96.4 W in our investigation and 48.7 W in the investigation of Yamamoto et al [6], a difference that may have been a cause of the discrepancy in frequency of microbubbles observed. In the present study, the number of HITS increased with the duration of radiofrequency current application. This may have resulted from the fact that the final temperature was higher with longer current application. The number of HITS also increased with tumour size, possibly because the volume of tissue in which coagulation occurred was greater, and the tissue therefore contained more fluid.

The present study had several limitations. Firstly, we did not differentiate between solid emboli and gas bubbles, and the small number of patients in this study makes it difficult to conclude that microbubbles have no effect on the cerebral circulation. Secondly, only the right internal carotid artery was examined in all patients. There is a possibility that microbubbles also flow in the left internal carotid artery, as well as in vertebral arteries. In addition, the probability of this flow might also depend upon the position of the patient during the ablation.

In conclusion, microbubbles were detected in all patients in the late phase of the first session of RFA.

References

1. Kruskal JB, Oliver B, Huertas JC, Goldberg SN. Dynamic intrahepatic flow and cellular alterations during radiofrequency ablation of liver tissue in mice. J Vasc Interv Radiol 2001;12:1193–201.
2. Livraghi T, Goldberg SN, Lazzaroni S, Meloni F, Solbiati L, Gazella GS. Small hepatocellular carcinoma: treatment with radio-frequency ablation versus ethanol injection. Radiology 1999;210:655–61.

3. Livraghi T, Goldberg SN, Lazzaroni S, Meloni F, Ierace T, Solbiati L, et al. Hepatocellular carcinoma: radio-frequency ablation of medium and large lesions. Radiology 2000;214:761–8.
4. Malone DE, Lesiuk L, Brady AP, Wyman DR, Wilson BC. Hepatic interstitial laser photocoagulation: demonstration and possible clinical importance of intravascular gas. Radiology 1994;193:233–7.
5. Rose SC, Fotoohi M, Levin DL, Harrell H. Cerebral microembolization during radiofrequency ablation of lung malignancies. J Vasc Interv Radiol 2002;13:1051–4.
6. Yamamoto A, Matsuoka T, Toyoshima M, Okuma T, Oyama Y, Hamuro M, et al. Assessment of cerebral microembolism during percutaneous radiofrequency ablation of lung tumors using diffusion-weighted imaging. AJR Am J Roentgenol 2004;183:1785–9.
7. Consensus Committee of the Ninth International Cerebral Hemodynamic Symposium. Basic identification criteria of doppler microembolic signals. Stroke 1995;26:1123.
8. Markus H, Loh A, Israel D, Buckenham T, Clifton A, Brown MM. Microscopic embolism during cerebral angiography and strategies for its avoidance. Lancet 1993;341:784–7.
9. Russell D, Madden KP, Clark WM, Sandset PM, Zivin JA. Detection of arterial emboli using Doppler ultrasound in rabbits. Stroke 1991;22:253–8.

ORIGINAL ARTICLE

ACTA RADIOLOGICA

Transcatheter Coil Embolization for Steal Syndrome in Patients with Hemodialysis Access

S. KARIYA[1], N. TANIGAWA[1], H. KOJIMA[1], A. KOMEMUSHI[1], Y. SHOMURA[1], T. SHIRAISHI[2], T. KAWANAKA[3] & S. SAWADA[1]

[1]Department of Radiology, Kansai Medical University, Osaka, Japan, [2]Department of Radiology and [3]Department of Urology, Ishikiri Seiki Hospital, Osaka, Japan

Kariya S, Tanigawa N, Kojima H, Komemushi A, Shomura Y, Shiraishi T, Kawanaka T, Sawada S. Transcatheter coil embolization for steal syndrome in patients with hemodialysis access. Acta Radiol 2009;50:28–33.

Background: Drainage of large amounts of shunt blood into deep veins via collaterals reduces resistance to venous outflow and decreases blood flow to the artery distal to the arterial anastomotic site, potentially resulting in steal syndrome.

Purpose: To evaluate the effectiveness of transcatheter coil embolization for collateral veins of hemodialysis access in the treatment of steal syndrome.

Materials and Methods: Five hemodialysis patients (four male, one female; mean age 58.8 years, range 40–71 years) with symptomatic steal syndrome were treated. Steal syndrome was diagnosed based on decreased or absent distal pulse, coolness, pain, abnormal skin color, ischemic ulceration of digits, numbness, sensory impairment, or motor impairment. Coil embolization was performed to block collaterals communicating with deep veins, with conscious sedation and local anesthesia. Fistulography was performed before, immediately after, and 1 month after embolization. Ultrasonography was performed 2 days after embolization. Symptoms and signs were assessed 2 days after embolization. Clinical findings related to steal syndrome and access failure were observed at each hemodialysis.

Results: Blood flow in the collaterals was successfully blocked by coil embolization in all patients. Distal pulse, coolness, pain, and skin color improved in all patients. Numbness, sensory impairment, and motor impairment were unimproved in two patients. In all patients, hemodialysis following embolization was performed normally. The mean observation period after embolization was 33 months (range 9–75 months).

Conclusion: Coil embolization of collaterals that drain shunt blood into deep veins is effective for steal syndrome for hemodialysis access originating in the brachial artery.

Key words: Adults; embolization; interventional; ischemia; vascular; vein

Shuji Kariya, Department of Radiology, Kansai Medical University, 2-3-1 Shinmachi, Hirakata, Osaka, 573-1192, Japan (tel. +81 72 804 0101, fax. +81 72 804 2865, e-mail. shauji@ops.dti.ne.jp)

Accepted for publication September 30, 2008

About 1% of patients with distal forearm arteriovenous (AV) fistulas and about 3–6% of patients with AV fistulas or AV grafts originating in the brachial artery display severe ischemic symptoms requiring treatment (1–5). Several surgical treatments have been devised for treatment of distal ischemia, such as access ligation, banding, and distal revascularization-interval ligation (6–8). Access ligation and banding are widely used. The banding technique is based on the concept that increasing resistance to fistula outflow will result in increased flow in the portion of the artery distal to the fistula (6, 7). The problem with this procedure is the difficulty in determining the required amount of stenosis.

Drainage of large amounts of shunt blood into deep veins via collaterals reduces resistance to fistula outflow and decreases blood flow to the artery distal to the arterial anastomotic site. Our therapeutic technique for steal syndrome is to block collaterals draining into deep veins that are unsuitable as hemodialysis access using coil embolization, and the basic concept behind this technique is to increase resistance to fistula outflow, as in surgical banding (6, 7).

informa
healthcare

DOI 10.1080/02841850802537933

The purpose of our study was to evaluate the effectiveness of transcatheter coil embolization for collateral veins of hemodialysis access in the treatment of steal syndrome.

Material and Methods

All study protocols were approved by our institutional review board, and written informed consent was obtained from all patients prior to participation. The present study was conducted from November 2001 to February 2008 in our institution, which has the capacity to provide hemodialysis to 400 chronic renal failure patients.

Patients and inclusion criteria

Five patients (four male, one female; mean age 58.8 years, range 40–71 years) were treated. Their characteristics, symptoms, and signs are shown in Table 1. Patients with chronic renal failure who satisfied the following inclusion criteria were enrolled in the study: 1) presence of AV fistulas or AV grafts originating in the brachial artery for hemodialysis; 2) diagnosis of steal syndrome; 3) access displaying collaterals shunting blood into deep veins that could not be used for hemodialysis access; and 4) manual compression of collaterals restores distal pulses by palpation.

Steal syndrome was diagnosed based on symptoms and signs, as defined by decreased or absent distal pulse, coolness, pain, abnormal skin color, ischemic ulceration of digits, numbness, sensory impairment, or motor impairment. Bedside palpation and auscultation were performed to confirm the existence of an outflow vein to be used as hemodialysis access (main outflow vein) and collaterals that drained into deep veins that were unsuitable for hemodialysis access. Collateral outflow veins were manually compressed, and restoration of distal pulses was confirmed by palpation.

In all patients, before the current hemodialysis access was created, hemodialysis was performed using an AV fistula created on the ipsilateral forearm. When this hemodialysis access failed, the current AV fistula or graft originating in the brachial artery was created.

Procedures

All procedures were performed on an outpatient basis with conscious sedation (midazolam; Yamanouchi Pharmaceutical, Tokyo, Japan).

In all patients, a 5F introducer sheath (Medikit, Miyazaki, Japan) was placed in the outflow vein or

Table 1. Patients and symptoms

Patient	1	2	3	4	5
Age, years	40	50	71	65	69
Sex	M	M	F	M	M
Diabetes	+	+	–	–	–
Type of access	AVF	AVF	AVG	AVF	AVF
Kind of anastomosis	Brachiocephalic AVF	Brachiocephalic AVF	Brachiobasilic AVG	Brachiocephalic AVF	Brachiobasilic AVF
Localization of anastomosis	Elbow	Elbow	Elbow	Elbow	Elbow
Current access age, days	34	65	123	1084	1283
Detection of brachial artery distal to the AV fistula in fistulography	–	–	•	–	–
Limb ischemia					
Decreased or absent distal pulses	+	+	+	+	+
Coolness	+	+	+	+	+
Pain during dialysis	+	+	+	+	+
Rest pain	+	+	+	+	+
Skin color	cyanosis	pallor	pallor	cyanosis	cyanosis
Ischemic ulcers	–	–	–	–	+
Gangrene	–	–	–	–	–
Neuropathy					
Numbness	+	+	–	–	–
Sensory impairment	+	+	–	–	–
Motor impairment	+	+	–	–	–

• Patient 3 underwent anterograde fistulography by injecting contrast medium from the graft.
AVF: arteriovenous fistula; AVG: arteriovenous graft.

graft, with local anesthesia of 1% lidocaine hydrochloride (Xylocaine polyamp 1%; AstraZeneca, Osaka, Japan). Anterograde fistulography was obtained before coil embolization (Ultimax MSDX R0042EAD; Toshiba Medical Systems, Tochigi, Japan). At fistulography, contrast medium (370 mg I/ml Iopamiron; Nihon Schering, Osaka, Japan) was injected through a 21G elastor needle placed in the brachial artery or through a 5F introducer sheath in the graft. Fistulography findings were matched with the collateral outflow vein detected by bedside palpation and auscultation, and the collateral outflow vein was manually compressed again to confirm restoration of distal pulses by palpation. The collateral outflow vein was identified and catheterized selectively in all patients using a 5F catheter (Fansac; Clinical Supply, Gifu, Japan) or with a coaxially placed microcatheter (2.7F progreat [Terumo, Tokyo, Japan] or Tracke 18 [Boston Scientific, Natick, Mass., USA]) advanced through the 5F catheter. Additional coils were placed in the collateral outflow vein until shunt blood stopped draining into deep veins. If multiple collateral outflow veins displayed high levels of blood flow, as many veins as necessary were embolized. Collateral outflow veins with low blood flow were left untouched. Pushable fibered coils were used in four patients, while detachable coils were used in one patient.

Pushable fibered coils were 0.38" Fibered Platinum Embolization Coils (Boston Scientific, Natick, Mass., USA), 5–9 mm in unconstrained diameter; FPC35 VORTX -35 Vascular Occlusion Coils (Boston Scientific, Natick, Mass., USA), 5–6 mm in unconstrained diameter; TORNADO MWCE-35 embolization coils (Cook, Bloomington, Ind., USA), 8 mm in unconstrained diameter; or VORTX-18 Diamond Shape Coils (Boston Scientific, Natick, Mass., USA), 5–6 mm in unconstrained diameter. We used pushable coils with nominal diameters 10–40% larger than estimated diameter of the collateral outflow vein (i.e., oversizing).

In one patient, the diameter of the collateral outflow vein gradually increased downstream toward the deep veins from the location of coil placement. As coil migration was a possibility, DCS-18S-SPIRAL detachable coils (Cook, Bloomington, Ind., USA) of 6–14 mm in unconstrained diameter were used with a DLD-11/18-UNI detach locking device (Cook, Bloomington, Ind., USA).

In patient 1 alone, blood pressure in the anastomotic site was measured before and after coil embolization. After the procedure, blood pressure was measured to evaluate whether hemodialysis following coil embolization was normal or not. Symptoms and signs 2 days after coil embolization were also assessed. In all patients, ultrasonography was performed 2 days after coil embolization and fistulography was performed 1 month after coil embolization. Clinical findings related to steal syndrome and access failure were observed at each hemodialysis.

Complications were categorized as minor or major according to the published guidelines of the Society of Interventional Radiology (9).

Results

In all patients, blood flow in collateral outflow veins was successfully blocked by transcatheter coil embolization (Fig. 1). Table 2 shows the results after coil embolization. In patient 1, blood pressure at the anastomotic site was 61/39 mmHg before coil embolization and 101/54 mmHg after embolization.

In all patients, fistulography 1 month after coil embolization showed that blood flow in the coil-embolized collateral outflow veins was still blocked. In patients 1–4, no new collateral outflow veins were seen, while patient 5 showed some new collaterals that were thin and superficial. In patient 3, fistulography showed that, 1 month after coil embolization, the main outflow vein was enlarged compared to before coil embolization. In patient 1, fistulography was performed 33 months after coil embolization, as the venous pressure in the main outflow vein increased. On fistulography, the main outflow vein was enlarged and stenosis of the central region of the main outflow vein was confirmed. This stenosis was dilated by balloon angioplasty.

Patient 5 recovered from the ulcer without administration of prostaglandin 1 month after coil embolization. In patient 1, numbness and motor and sensory impairments gradually improved after coil embolization and resolved completely within 18 months. In patient 2, numbness and motor and sensory impairments had not improved 9 months after coil embolization. As a result, the AV fistula was surgically ligated 288 days after coil embolization, and superficialization of the brachial artery was performed on the contralateral upper arm. However, numbness and motor and sensory impairments were unimproved soon after ligation. The main outflow vein remained patent for 75 months in patient 1, 37 months in patient 3, 21 months in patient 4, and 24 months in patient 5. In all patients, ischemia of the limb distal to AV fistula or graft site did not recur.

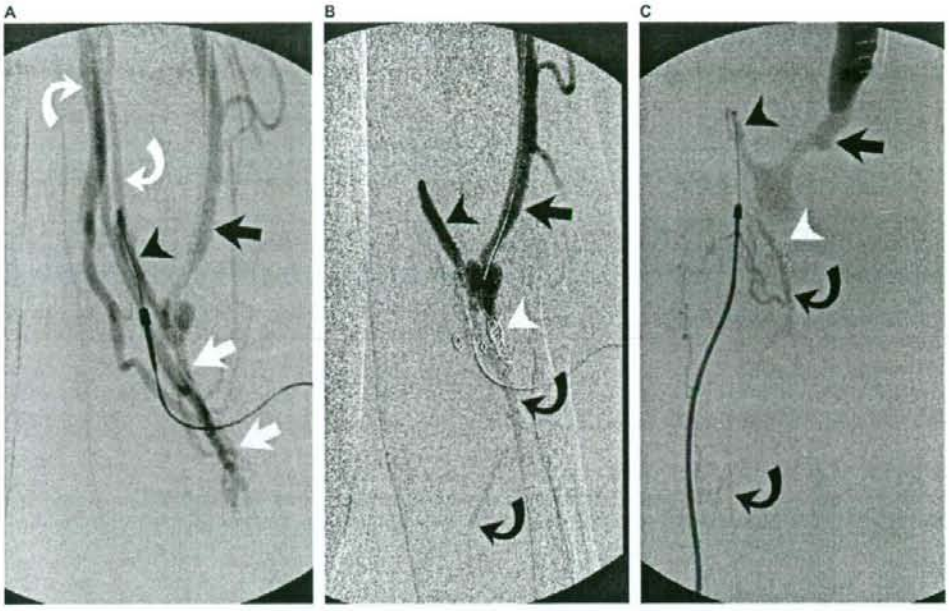

Fig. 1. Patient 1. Fistulography in a 40-year-old man displaying steal syndrome with AV fistula originating in the brachial artery. All figures were obtained by anterograde fistulography, and contrast medium was injected through a 21G elastor needle placed in the brachial artery (black arrowheads). A. Fistulography before coil embolization. Beside the main outflow vein used as hemodialysis access (black arrow), collateral outflow veins (white arrows) drained shunt blood into deep veins (curved white arrows). The artery distal to the AV fistula site could not be depicted. B. Fistulography immediately after coil embolization. A coil (white arrowhead) was placed to embolize the collateral outflow vein. While drainage to deep veins was blocked, the main outflow vein (black arrow) was unaffected. Blood flow in the artery distal to the AV fistula site (curved black arrow) was weak but became anterograde. C. Fistulography following balloon angioplasty for main outflow vein stenosis at 33 months after coil embolization. Blood flow in the artery distal to the AV fistula site (curved black arrows) remained anterograde. The main outflow vein (black arrow) was dilated compared to at the time of coil embolization. The coil (white arrowhead) still blocked the collateral outflow vein.

In patients 3–5, minor complications of flare, pain, and heat sensation at the site of embolization were present starting on the day of coil embolization, and lasted for 3–8 days. Symptoms were limited to coil-embolized collateral outflow veins and improved without medication. No patients experienced coil migration during or after coil embolization, and no other complications were seen.

Discussion

As the patients in the present study had AV fistula on the ipsilateral forearm until the creation of the current hemodialysis access, collateral outflow and deep veins might have been dilated. In this state, shunt blood might be likely to drain into deep veins via collateral outflow veins bifurcating from main outflow veins near the anastomotic site, potentially reducing resistance to fistula outflow and decreasing blood flow in the artery distal to the arterial anastomotic site.

In our patients with shunt blood draining into deep veins, peripheral circulatory failure due to venous hypertension might represent one cause of hand ischemia. Although no typical clinical findings of venous hypertension were noted in our patients, it was not possible to clarify this in the study.

Symptoms attributable to ischemia improved in all patients, so transcatheter coil embolization of collateral outflow veins appears to offer a feasible method of treatment for steal syndrome. The basic concept of our technique is to increase resistance to fistula outflow, as seen with surgical banding (6, 7). In patient 1, blood pressure at the anastomotic site increased immediately after coil embolization, suggesting increased resistance to fistula outflow.

The presence of a collateral outflow vein draining a large amount of shunt blood to deep veins was confirmed by bedside palpation and auscultation,

Table 2. Results after coil embolization

Patient	1	2	3	4	5
Number of coils used					
Pushable coils	5	5	7	0	20
Detachable coils	0	0	0	8	0
Detection of brachial artery distal to AV fistula in fistulography	+	+	*	+	−
Hemodialysis after coil embolization	normal	normal	normal	normal	normal
Limb ischemia					
Decreased or absent distal pulses	−	−	−	−	+
Coolness	−	−	−	−	−
Pain during dialysis	−	−	−	−	−
Rest pain	−	−	−	−	−
Skin color	normal	normal	normal	normal	normal
Ischemic ulcers	−	−	−	−	−
Gangrene	−	−	−	−	−
Neuropathy					
Numbness	+	+	−	−	−
Sensory impairment	+	+	−	−	−
Motor impairment	+	+	−	−	−

* Patient 3 underwent anterograde fistulography, by injecting contrast medium from the graft.
AV: arteriovenous.

and we determined whether to perform coil embolization by manually compressing the collateral outflow vein. Selection of patients meeting the indications for our method of treatment before fistulography thus appears feasible.

The reason for using detachable coils in one patient was that coil migration was possible based on location and blood flow. In this patient, coils were placed over the bifurcation for multiple collateral outflow veins. When the diameter of collateral outflow veins gradually increases downstream toward the deep veins, the risk of coil migration requires attention.

In two patients, numbness and motor and sensory impairments did not improve immediately after coil embolization. These cases appear to have involved ischemic monomelic neuropathies that were irreversible (10–13).

Enlargement of the main outflow vein was confirmed in two patients (40%). As a result, our technique may have excessively developed the main outflow vein. One patient displayed increased venous pressure 33 months after coil embolization due to stenosis of the central region of the main outflow vein. This might have been attributable to blockage of collaterals draining shunt blood into deep veins, thus increasing blood flow in the main outflow vein.

Fever, pain, and flare in three patients after coil embolization were typical symptoms of thrombophlebitis. Thrombotic occlusion was not seen in veins by ultrasonography, excluding embolized veins. We will thus be able to use the brachial or basilic vein as a drainage vein when new surgical reconstruction of hemodialysis access becomes necessary.

One advantage of our technique is that the same hemodialysis access used before therapy can be used without lowering blood flow in the main outflow vein. Conversely, banding lowers blood flow in the main outflow vein. Adjustment of the blood flow by banding is difficult and may cause thrombosis of hemodialysis access (14, 15).

We did not evaluate quantitatively the results before and after embolization. However, quantitative evaluation of blood flow and digital pressure may be done for an objective evaluation of the treatment results (16, 17). Our technique is unsuitable for steal syndrome in which excessive shunt blood is drained into the collateral outflow vein for access, because access could be lost following embolization.

In conclusion, coil embolization of collaterals that drain shunt blood into deep veins that cannot be used for hemodialysis access is effective for steal syndrome associated with AV fistula or graft originating in the brachial artery.

Declaration of interest: The authors report no conflicts of interest. The authors alone are responsible for the content and writing of the paper.

References

1. Duncan H, Ferguson L, Faris I. Incidence of the radial steal syndrome in patients with Brescia fistula for hemodialysis: its clinical significance. J Vasc Surg 1986; 4:144–7.
2. Haimov M, Burrows L, Schanzer H, Neff M, Baez A, Kwun K, et al. Experience with arterial substitutes in the construction of vascular access for hemodialysis. J Cardiovasc Surg (Torino) 1980;21:149–54.
3. Porter JA, Sharp WV, Walsh EJ. Complications of vascular access in a dialysis population. Curr Surg 1985; 42:298–300.
4. Zibari GB, Rohr MS, Landreneau MD, Bridges RM, DeVault GA, Petty FH, et al. Complications from permanent hemodialysis vascular access. Surgery 1988; 104:681–6.
5. Winsett OE, Wolma FJ. Complications of vascular access for hemodialysis. South Med J 1985;78:513–7.
6. Corry RJ, Patel NP, West JC. Surgical management of complications of vascular access for hemodialysis. Surg Gynecol Obstet 1980;151:49–54.
7. Morsy AH, Kulbaski M, Chen C, Isiklar H, Lumsden AB. Incidence and characteristics of patients with hand ischemia after a hemodialysis access procedure. J Surg Res 1998;74:8–10.
8. Berman SS Gentile AT Glickman MH Mills JL Hurwitz RL Westerband A et al. Distal revascularization-interval ligation for limb salvage and maintenance of dialysis access in ischemic steal syndrome. J Vasc Surg 1997;26:393–402; discussion 402.
9. Aruny JE, Lewis CA, Cardella JF, Cole PE, Davis A, Drooz AT, et al. Quality improvement guidelines for percutaneous management of the thrombosed or dysfunctional dialysis access. Standards of Practice Committee of the Society of Cardiovascular & Interventional Radiology. J Vasc Interv Radiol 1999;10: 491–8.
10. Bolton CF, Driedger AA, Lindsay RM. Ischaemic neuropathy in uraemic patients caused by bovine arteriovenous shunt. J Neurol Neurosurg Psychiatry 1979;42:810–4.
11. Wilbourn AJ, Furlan AJ, Hulley W, Ruschhaupt W. Ischemic monomelic neuropathy. Neurology 1983;33: 447–51.
12. Hye RJ, Wolf YG. Ischemic monomelic neuropathy: an under-recognized complication of hemodialysis access. Ann Vasc Surg 1994;8:578–82.
13. Redfern AB, Zimmerman NB. Neurologic and ischemic complications of upper extremity vascular access for dialysis. J Hand Surg [Am] 1995;20:199–204.
14. Ebeid A, Saranchak HJ. Banding of a PTFE hemodialysis fistula in the treatment of steal syndrome. Clin Exp Dial Apheresis 1981;5:251–7.
15. Dally P, Brantigan CO. Plethysmography and the diagnosis of the steal syndrome following placement of arteriovenous fistulas and shunts for hemodialysis access. J Cardiovasc Surg (Torino) 1987;28:200–3.
16. Wixon CL, Hughes JD, Mills JL. Understanding strategies for the treatment of ischemic steal syndrome after hemodialysis access. J Am Coll Surg 2000;191: 301–10.
17. Schanzer H, Eisenberg D. Management of steal syndrome resulting from dialysis access. Semin Vasc Surg 2004;17:45–9.

Cardiovasc Intervent Radiol (2008) 31:86–90
DOI 10.1007/s00270-007-9189-0

CLINICAL INVESTIGATION

Hepatic Arterial Infusion Chemotherapy through a Port-Catheter System as Preoperative Initial Therapy in Patients with Advanced Liver Dysfunction due to Synchronous and Unresectable Liver Metastases from Colorectal Cancer

Toshihiro Iguchi · Yasuaki Arai · Yoshitaka Inaba · Hidekazu Yamaura · Yozo Sato · Masaya Miyazaki · Hiroshi Shimamoto

Received: 5 June 2007 / Accepted: 11 September 2007 / Published online: 10 October 2007

Abstract
Purpose We retrospectively evaluated the safety and efficacy of preoperative initial hepatic arterial infusion chemotherapy (HAIC) through a port-catheter system in patients with liver dysfunction due to synchronous and unresectable liver metastases. The aim of HAIC was to improve patients' clinical condition for later surgical removal of primary colorectal cancer.
Methods Port-catheter systems were placed radiologically in 21 patients (mean age 58.6 ± 8.1 years) with liver dysfunction due to synchronous liver metastases from colorectal cancer. Initial HAIC of 1,000 mg/m^2 5-fluorouracil was administered weekly as a 5 hr continuous infusion through this system. Surgical removal of the primary lesion was planned after HAIC improved the liver function.
Results Port-catheter system placement was successful in all patients without severe complications. Patients were followed up for a median of 309 days (range 51–998 days). After starting HAIC, no severe adverse events that caused drug loss and treatment postponement or suspension were observed in any of the patients. HAIC was performed a mean of 4.5 ± 3.0 times and the liver function improved in all patients. Curative (n = 18) or palliative (n = 1) surgical removal of the primary lesion was performed. The remaining 2 patients died because extrahepatic metastases developed and their performance status worsened; thus, surgery could not be performed. The median survival times of all patients and the operated patients were 309 and 386 days, respectively.
Conclusion Initial HAIC administration is a safe and efficacious method for improving liver function prior to operative resection of primary colorectal cancer in patients with liver dysfunction due to synchronous and unresectable liver metastases.

Keywords Colorectal cancer · Hepatic arterial infusion chemotherapy · Liver metastasis · Port-catheter system

Introduction

Colorectal cancer is the fourth most commonly diagnosed malignant disease worldwide [1], and synchronous liver metastases are identified in 10–20% of cases [2]. However, the treatment protocol for patients with stage IV colorectal cancer with synchronous liver metastases has not been firmly established [2, 3]. In such patients, the choice of treatment strategy differs based on various factors such as liver function, the patient's condition, the urgency of operating on the primary lesion, and the institution's protocols for dealing with liver metastases and primary lesions. For the primary lesion, it is desirable that surgical removal is selected to improve the quality of life of the patients, because colorectal cancer may cause obstruction, perforation, bleeding, or pain [3]. Additionally it has been reported that stage IV patients who underwent resection of their asymptomatic primary lesions had prolonged median and 2-year survival periods compared with stage IV

T. Iguchi · Y. Inaba (✉) · H. Yamaura · Y. Sato · M. Miyazaki · H. Shimamoto
Department of Diagnostic and Interventional Radiology, Aichi Cancer Center Hospital, 1-1 Kanokoden, Nagoya, Chikusa-ku 464-8681, Japan
e-mail: 105824@aichi-cc.jp

Y. Arai
Department of Diagnostic Radiology, National Cancer Center Hospital, 5–1–1, Tsukiji, Tokyo, Chuo-ku 104–0045, Japan

was inserted from the left subclavian artery and advanced to the common hepatic artery via the celiac artery. Then an indwelling catheter (Anthron P-U catheter; Toray Medical, Tokyo, Japan or W spiral catheter; PIOLAX, Yokohama, Japan) with a side hole was inserted using the catheter-exchange method. The catheter tip was inserted into the deep segment of the gastroduodenal artery so that the side hole was placed into the common hepatic artery. The gastroduodenal artery around the tip of the indwelling catheter was embolized using microcoils and a mixture (1:1.5) of *n*-butyl cyanoacrylate (NBCA; Histoacryl; Braun, Melsungen, Germany) and iodized oil (Lipiodol Ultrafluide; Laboratoire Guerbet, Roissy, France) through a microcatheter inserted coaxially via the 5 Fr angiographic catheter inserted from the right femoral artery. Finally, the proximal end of the indwelling catheter was connected to a port implanted in the subcutaneous pocket created in the left chest wall.

Digital subtraction angiography and CT were performed during injection of contrast medium through the implanted port-catheter system within a few days of implantation to confirm that the catheter was not dislodged and that the entire liver was perfused adequately. Thereafter, HAIC was administered through this system: 1,000 mg/m^2 of 5-fluorouracil (5-FU) weekly by continuous 5 hr infusion [7]. After administration of the chemotherapeutic agent, the implanted port-catheter system was flushed and filled with 2 ml of heparin solution (1,000 IU/ml).

Statistical Analysis

The success rate and the complications of the placement of the port-catheter system were evaluated. After starting HAIC the clinical course, including improvement in liver function tests, performance of surgery, and survival were evaluated. In patients who underwent surgical removal of the primary lesion, the frequency of HAIC administration, time between the placement of the port-catheter system and surgery, details of the surgery, postoperative therapy, and survival were evaluated. The Wilcoxon signed rank test was used to compare the liver functions before surgery with those before starting HAIC. The cumulative survival rate was calculated using the Kaplan-Meier method.

A p value of less than .05 was considered significant.

Results

After placement of the port-catheter system, patients were followed up for a median of 309 days (range 51–998 days).

Placement of the Port-Catheter System

The radiological placement of the port-catheter system was successful in all 21 patients. During and after the procedure, there were no complications such as hematoma, subclavian or vertebral artery thrombosis, infections, hepatic artery occlusions, and catheter malfunctions.

Clinical Course after Starting HAIC

After starting HAIC, no severe adverse events that caused drug loss and treatment postponement or suspension were observed in any of the patients. HAIC was performed a mean of 4.5 ± 3.0 times (range 1–15 times) and the liver function improved in all 21 patients. In particular, the AST, ALT, LDH, ALP, and GTP levels were improved significantly (Table 1). In 19 of 21 patients, curative (n = 18) or palliative (n = 1) surgical removal of the primary lesion was performed. In the remaining 2 patients, although the liver function had improved after HAIC was administered 15 times and 5 times, respectively, extrahepatic metastases in the lung, bone or peritoneum developed rapidly and their performance status worsened. Though systemic chemotherapy was administered with or instead of HAIC afterward, they died 186 and 51 days, respectively, after the placement of port-catheter system; thus, surgery could not be performed.

Among the 19 patients who underwent surgery, HAIC was administered a mean of 3.9 ± 1.8 times (range 1–9 times), and the median period between placement of the

Table 1 Liver function before and after HAIC administration

		Before starting HAIC	After HAIC	p value
AST (IU/l)	Mean	110 ± 109	56 ± 55	
	Range	21–549	21–273	0.0001*
ALT (IU/l)	Mean	59 ± 43	31 ± 22	
	Range	17–183	11–101	0.0005*
T-BIL (mg/dl)	Mean	1.0 ± 0.5	1.2 ± 1.1	
	Range	0.3–2.2	0.3–4.4	0.717
LDH (IU/l)	Mean	1242 ± 1002	551 ± 501	
	Range	221–3870	174–2050	<0.0001*
ALP (IU/l)	Mean	874 ± 570	663 ± 526	
	Range	416–2660	124–2335	0.0046*
GTP (IU/l)	Mean	393 ± 433	207 ± 169	
	Range	130–2023	9–602	0.0061*

AST, aspartate aminotransferase; ALT, alanine aminotransferase; T-BIL, total bilirubin; LDH, lactate dehydrogenase; ALP, alkaline phosphatase; GTP, gamma-glutamyl transpeptidase; HAIC, hepatic arterial infusion chemotherapy

*Significant at $p < 0.05$

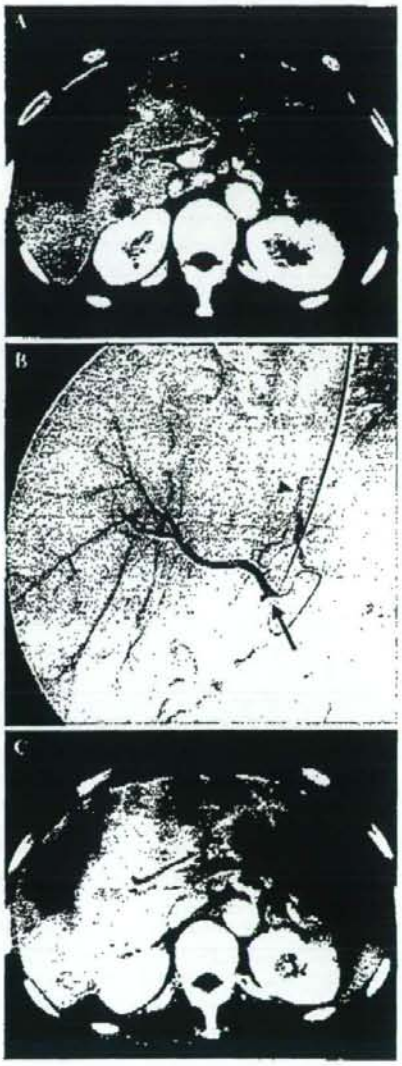

Fig. 2 A–C. A 55-year-old man with multiple liver metastases from rectal cancer. A Contrast-enhanced CT scan obtained before starting HAIC shows unresectable multiple liver metastases in both the right and left lobes. B An arteriogram via the port obtained before starting HAIC shows that all hepatic arteries are well visualized. The catheter tip was inserted into the deep segment of the gastroduodenal artery and embolized using microcoils and a mixture of *n*-butyl cyanoacrylate and iodized oil. The side hole was placed into the common hepatic artery (arrow). The accessory left hepatic artery, which branched from the left gastric artery, was embolized with microcoils (arrowhead) in order to establish hepatic arterial supply from a single vessel. C Contrast-enhanced CT scan obtained after five HAIC administrations shows slightly smaller multiple liver metastases. With the exception of T-BIL, the patient's liver function improved (AST improved from 83 to 26 IU/l, ALT improved from 49 to 18 IU/l, LDH improved from 1,155 to 458 IU/l, and ALP improved from 950 to 502 IU/l)

port-catheter system and surgery was 29 days (range 14–68 days). Of 13 patients who had no extrahepatic metastases prior to the surgery, 10 developed extrahepatic metastases. Among 16 of 19 patients, systemic chemotherapy with or instead of HAIC was administered after the surgery.

The overall median survival time of all the patients was 309 days and that of the patients who underwent surgery was 386 days (Fig. 1). At present, 20 patients have died.

A representative case is shown in Fig. 2.

Discussion

Many studies have reported the effectiveness of HAIC administration through a port-catheter system for liver metastases from colorectal cancer [6–8]. In Western countries, it has been reported that HAIC is effective in treating liver metastases; however, it does not improve the prognosis [6]. On the other hand, in Japan, good results have been reported after intermittent hepatic arterial infusion of a high dose of 5-FU: the response rate is reportedly 78% and the median survival time is 25.8 months [7].

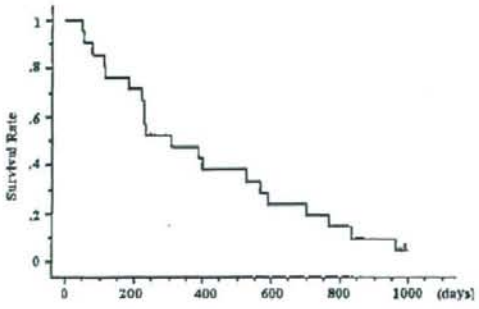

Fig. 1 Overall survival time

In general, systemic chemotherapy is usually selected for colorectal cancer with distant metastases [2]. Recently, the standard regimens such as FOLFILI (5-FU plus leucovorin with oxaliplatin) and FORFOX (5-FU plus leucovorin and irinotecan) are used, and the median survival after FOLFILI and FORFOX has been reported to be 12.6–21.5 months [12]. In many cases, systemic chemotherapy might be the first choice of treatment for patients with primary colorectal cancer and synchronous distant metastases, and we usually select systemic chemotherapy

as an initial therapy for such patients. Although it is doubtful whether the initial HAIC administration is effective in patients who have not undergone any therapy for the primary lesion, HAIC was administered initially in order to improve or control liver metastases. We judged that liver metastasis was the prognosis-limiting factor, because the liver dysfunction in these patients had already progressed due to liver metastases. Additionally, we aim to surgically remove the primary lesion later, if possible, because primary colorectal cancer may cause obstruction, perforation, bleeding, or pain [3]. Based on the results of this study, we believe that initial HAIC administration is effective because, in 19 of 21 patients, surgery was possible after the liver function had been improved by HAIC administration.

In the 19 patients who underwent surgery, HAIC administration was terminated 1 week before surgery to prevent its effect on surgery. The wide range of the frequency of HAIC administration was due to the fact that surgery was not performed until, in the surgeons' opinion, the patient's liver function had improved. We observed that the liver functions before surgery had improved significantly after HAIC administration compared with those before starting HAIC. It has been reported that HAIC has fewer side effects than systemic chemotherapy [13] and, in fact, we observed that surgeries could be performed without any adverse effects arising due to HAIC. We usually consider T-BIL >3.0 mg/dl or a performance status of 4 as the exclusion criteria for HAIC administration because, based on our experience, it is difficult to reduce such liver dysfunction and also improve performance status in patients. Further, the liver dysfunction of such patients may be adversely affected by HAIC administration. Based on our results, there were no severe adverse events after HAIC administration when these exclusion criteria were used for the selection of the candidates. In 2 of 21 patients, although the liver function improved after HAIC administration, surgery could not be performed because they developed extrahepatic metastases in the lung, bone or peritoneum, and their performance status worsened. Unfortunately, we cannot expect HAIC administration to have an anticancer effect on the entire body [7].

There were some limitations in our retrospective study. Firstly, the liver dysfunction of our patients was already advanced; therefore, we hesitated to administer systemic chemotherapy when malignancy was first identified. Secondly, in many patients, other distant metastases were present or developed and systemic chemotherapy was started after the surgery. We could not administer standard systemic chemotherapy such as FOLFILI and FORFOX, and our regimens of systemic chemotherapy were not established, because it is only recently that such standard regimens have been employed in practice in Japan. The survival period might have been prolonged if we had employed the currently used standard systemic chemotherapy.

In conclusion, initial HAIC administration is a safe and efficacious method for improving liver function prior to operative resection of primary colorectal cancer in patients with liver dysfunction due to synchronous and unresectable liver metastases.

References

1. Ferlay J, Bray F, Pisani P, Parkin DM (2004) GLOBOCAN 2002: Cancer incidence, mortality and prevalence worldwide. IARC CancerBase no. 5, version 2.0. IARC Press, Lyon, France
2. Alexander HR, Kemeny NE, Lawrence TS (2000) Metastatic cancer to the liver. In: DeVita VT (ed) Cancer, 7th edn. Williams & Wilkins, Baltimore, pp 2353–2368
3. Ruo L, Gougoutas C, Paty PB, et al. (2003) Elective bowel resection for incurable stage IV colorectal cancer: Prognostic variables for asymptomatic patients. J Am Coll Surg 196:722–728
4. Tanaka T, Arai Y, Inaba Y, et al. (2003) Radiologic placement of side-hole catheter with tip fixation for hepatic arterial infusion chemotherapy. J Vasc Interv Radiol 14:63–68
5. Yamagami T, Iida S, Kato T, et al. (2002) Using *n*-butyl cyanoacrylate and the fixed-catheter-tip technique in percutaneous implantation of a port-catheter system in patients undergoing repeated hepatic arterial chemotherapy. AJR Am J Roentgenol 179:1611–1617
6. Meta-Analysis Group in Cancer (1996) Reappraisal of hepatic arterial infusion in the treatment of nonresectable liver metastases from colorectal cancer. J Natl Cancer Inst 88:252–258
7. Arai Y, Inaba Y, Takeuchi Y, et al. (1997) Intermittent hepatic arterial infusion of high-dose 5FU on a weekly schedule for liver metastases from colorectal cancer. Cancer Chemother Pharmacol 40:526–530
8. Link KH, Sunelaitis E, Kornmann M, et al. (2001) Regional chemotherapy of nonresectable colorectal liver metastases with mitoxantrone, 5-fluorouracil, folinic acid, and mitomycin C may prolong survival. Cancer 92:2746–2753
9. Oken MM, Creech RH, Tormey DC, et al. (1982) Toxicity and response criteria of the Eastern Cooperative Oncology Group. Am J Clin Oncol 5:649–655
10. Arai Y, Inaba Y, Takeuchi Y (1997) Interventional techniques for hepatic arterial infusion chemotherapy. In: Castaneda-Zuniga WR (ed) Interventional radiology, 3rd edn. Williams & Wilkins, Baltimore, pp 192–205
11. Inaba Y, Arai Y, Matsueda K, et al. (2001) Right gastric artery embolization to prevent acute gastric mucosal lesions in patients undergoing repeat hepatic arterial infusion chemotherapy. J Vasc Interv Radiol 12:957–963
12. Kelly H, Goldberg RM (2005) Systemic therapy for metastatic colorectal cancer: Current options, current evidence. J Clin Oncol 23:4553–4560
13. Collins JM (1984) Pharmacokinetic rationale for intra-arterial therapy. In: Howell SB (ed) Intra-arterial and intracavitary cancer chemotherapy. Martinus Nijhoff, Boston, pp 1–10

Original Research

Equivalent Cross-Relaxation Rate Imaging of Axillary Lymph Nodes in Breast Cancer

Shigeru Mastsushima, RT, PhD,[1*] Hideyuki Nishiofuku, MD,[2] Hiroji Iwata, MD, PhD,[3] Seiichi Era, MD, PhD,[4] Yoshitaka Inaba, MD, PhD,[5] and Yasutomi Kinosada, MD, PhD[1]

Purpose: To determine whether equivalent cross-relaxation rate (ECR) imaging (ECRI) is a feasible method for optimization of axillary lymph node dissection (ALND) and thereby improve quality-of-life (QOL).

Materials and Methods: A total of 50 breast cancer patients underwent ECRI, with off-resonance saturation pulse at frequency offset of 5 ppm. ECR threshold values were determined to evaluate metastases to lymph nodes in the ALND group before examining the relationship between ECR value and cellular density. Metastases to lymph nodes of the sentinel lymph node biopsy (SLNB) group were evaluated based on the results of the ALND group.

Results: In the ALND group, regions without metastases showed a higher cellular density and ECR value than those with metastases. The relationship of ECR value to cellular density formed two clusters according to the presence or absence of metastasis; cellular density was related to ECR value for both clusters. In the SLNB group, supposing a threshold ECR value of 80%, sensitivity and specificity were 88.2% and 100%, respectively.

Conclusion: ECRI is a potentially useful method for cellular density imaging of axillary lymph nodes. ECRI provides active information that enables ALND to be avoided, thus improving QOL.

Key Words: sentinel lymph node; cellular imaging; molecular imaging; breast cancer; equivalent cross-relaxation rate; magnetization transfer
J. Magn. Reson. Imaging 2008;27:1278–1283.

LYMPHEDEMA IS A RELATIVELY COMMON, potentially serious, and unpleasant complication after axillary lymph node dissection (ALND) for breast cancer. It may be associated with functional, esthetic, and psychological problems, thereby affecting the quality-of-life (QOL) of breast cancer survivors. lymphedema also predisposes to the development of other secondary complications such as infections of the upper limb, psychological sequelae, development of malignant tumors, and deterioration in QOL (1). The risk of lymphedema is associated with the extent of ALND and the addition of axillary radiation therapy (1). Sentinel lymph node (SLN) biopsy (SLNB) is fast becoming the technique of choice for determining whether breast cancer has spread to lymph ducts or nodes. SNLB is only bypassed where significant evidence exists of clinical involvement of one or more axillary lymph nodes (2).

Molecular imaging is also instrumental in drug development, gene therapy, and in clinical research of breast cancer following the advent of fluorodeoxyglucose positron emission tomography and SLN techniques (3–5). While current methods are based on radio-lymphoscintigraphy (6), fluorescence lymphangiography (7) and magnetic resonance lymphangiography (MRL) (8) offer the benefits of improved spatial resolution without ionizing radiation. MRL is used for localizing SLNs in breast cancer; previous studies have reported the use of contrast agent (9–13).

In contrast, equivalent cross-relaxation rate (ECR) imaging (ECRI) is an MRI measurement method used to quantitatively evaluate a change in the protein–water interaction (14–18). Earlier studies further refined this technique and demonstrated that the cross-relaxation rate can be calculated using a simple equation; this was termed the ECR (14,15). In ECRI, the contrast obtained in breast cancer tissue has been shown to correlate with the malignant potential of cells and the extent of fibrosis (15,16).

It was reported that ECRI was related to changes in the macroscopic image and that it was possible to evaluate the presence or absence of axillary lymph node metastases using this technique (17,18). In the present study, we aimed to assess the precision of ECRI as a predictor of axillary lymph node metastasis to optimize ALND and improve QOL.

[1]Department of Biomedical Informatics, Gifu University Graduate School of Medicine, Gifu, Japan.
[2]Department of Radiology, Nara Medical University, Nara, Japan.
[3]Department of Breast Surgery, Aichi Cancer Center, Nagoya, Japan.
[4]Department of Physiology and Biophysics, Gifu University Graduate School of Medicine, Gifu, Japan.
[5]Department of Diagnostic and Interventional Radiology, Aichi Cancer Center, Nagoya, Japan.
Contract grant sponsor: JSPS, KAKENHI; Contract grant number: 19591409.
*Address reprint requests to: S.M., RT, PhD, Department of Biomedical Informatics, Gifu University Graduate School of Medicine, 1-1 Yanagido, Gifu 501-1194, Japan. E-mail: smts@gifu-u.ac.jp
Received July 30, 2007; Accepted February 7, 2008.
DOI 10.1002/jmri.21355
Published online in Wiley InterScience (www.interscience.wiley.com).